3B2v8.06a/w (Dec 5 2003).51c XML:ver:5.0.1 PSS : 1833 Prod.Type:FTP pp.1–12(col.fig.:1–10) ED:Asha PAGN:Raj SCAN:V4soft

ARTICLE IN PRESS

Available online at www.sciencedirect.com

SCIENCE DIRECT®

ELSEVIER

Planetary and Space Science ▮ (▮▮▮▮) 1–▮▮▮

Planetary and Space Science

www.elsevier.com/locate/pss

A three end-member model for petrologic analysis of lunar prospector gamma-ray spectrometer data

A.A. Berezhnoy[a,1], N. Hasebe[a], M. Kobayashi[a], G.G. Michael[b,*], O. Okudaira[a], N. Yamashita[a]

[a]*Advanced Research Institute for Science and Engineering, Waseda University, 3-4-1 Okubo, Shinjuku-ku, 169-8555 Tokyo, Japan*
[b]*German Aerospace Centre, Institute for Planetary Research, Rutherfordstr. 2, 12489 Berlin-Adlershof, Germany*

Received 24 March 2004; received in revised form 10 February 2005; accepted 20 February 2005

Abstract

We analyze preliminary Lunar Prospector gamma-ray spectrometer data. Al–Mg and Fe–Mg petrologic maps of the Moon show that Mg-rich rocks are located in Mare Frigoris, the South Pole Aitken basin, and in some cryptomaria. Analysis of distances of Lunar Prospector pixels from three end-member plane in Mg–Al–Fe space reveals existence of Ca-rich, Al-low small-area anomalies in the farside highlands. An Mg–Th–Fe petrologic technique can be used for estimation of abundances of ferroan anorthosites, mare basalts, KREEP basalts, and Mg-rich rocks.

Keywords: Moon; Gamma-ray spectroscopy; Petrologic mapping; Mg-rich rocks

1. Introduction

Elemental mapping of the Moon is very important for a better understanding of lunar formation and its evolutional history. Elemental maps of the Moon's surface make it possible to identify different types of mare basalts and petrologic units in the highlands, to determine the composition of ancient cryptomare and the South Pole Aitken basin, to search for regions with unusual chemical composition, and to estimate abundances of volatile elements at the lunar poles. Apollo X-ray and gamma-ray spectrometers determined the abundances of Fe, Th, and Al/Si and Mg/Si ratios for equatorial regions of the Moon. Using these data, Davis and Spudis (1985) established that all the observed elemental abundances could be explained by a mixing of ferroan anorthosite, mare basalts and KREEP basalts. Due to old volcanic eruptions and due to mixing by meteoroid impacts, mare basalts exist in the farside lunar highlands. Lucey et al. (1998) developed the Clementine spectral reflectance technique to map FeO and TiO_2 abundances within an error of about 1 wt%. Optical and near-infrared spectroscopy is useful and powerful for the determination of particle size, maturity, and content of minerals on the lunar surface (McCord et al., 1981; Shkuratov et al., 2003; Lucey, 2004).

Global mapping of Th and Fe abundances on the Moon was conducted using low-resolution gamma-ray spectra observed by Lunar Prospector (Lawrence et al., 1998, 2000, 2002, 2003). Among the results, the most interesting things were the mapping of the distribution of KREEP basalts on the lunar surface, the detection of geochemical anomalies at Tycho crater and in the Compton–Belkovich region, the estimation of the elemental composition of the South Pole Aitken basin, and the detection of small-area Th-rich anomalies. Preliminary data about other elements, including O, Si, Mg, Al, Ca, K, U, and Ti were presented by

*Corresponding author. Tel.: +49 30 67055369.
E-mail address: gregory.michael@dlr.de (G.G. Michael).
[1]Now at Sternberg Astronomical Institute, Universitetskij pr., 13, 119992 Moscow, Russia

0032-0633/$ - see front matter
doi:10.1016/j.pss.2005.02.006

Prettyman et al. (2002a), but a full analysis of these data is not finished yet.

In the near future, our knowledge about the elemental composition of the Moon will be greatly improved by the effort of few missions. The European SMART-1 mission carrying the AMIE camera for optical band photometry, an infrared spectrometer and an X-ray spectrometer started to observe the Moon in 2005. The X-ray spectrometer will map abundances of Al, Mg, Fe and Si (Dunkin et al., 2003), and the infrared spectrometer will be a powerful instrument for the detection of different minerals (Keller et al., 2001). The Japanese SELENE mission is scheduled for launch in 2006. The spacecraft carries gamma-ray and X-ray spectrometers. The X-ray spectrometer is planned to map Al, Mg, Fe, and Si abundance with a spatial resolution of 20 km (Okada et al., 2002). The SELENE gamma-ray spectrometer, employing a Ge detector with excellent energy resolution, will map Th, Fe, O, Si, Mg, Al, Ca, K, U, and Ti abundances (Kobayashi et al., 2002). In our article, we develop methods and approaches for analysis of the preliminary Lunar Prospector gamma-ray spectrometer data (Prettyman et al., 2002a).

2. Correlations between abundances of major elements on the Moon

Lunar Prospector gamma-ray spectrometer data give the abundances of 10 elements on the Moon with spatial resolution of 150 km, corresponding to a 5×5 degree area. Ti and K data are given with spatial resolution of 60 km, while Th and Fe data are given with 15 km pixel size (real spatial resolution is about 50 km). The quality of these data is good enough for preliminary analysis. For estimation of the quality of Lunar Prospector data, let us compare the elemental composition of landing sites measured by Lunar Prospector and by analysis of returned samples. This approach has some problems, among them difference between spatial resolution of Lunar Prospector measurements (50–150 km) and returned sample analysis (less than few kilometers) and the question of representativity of few studied lunar samples. The bulk composition of returned sample sites is taken according to Elphic et al. (2000). There are positive correlations between abundances of all elements, except Si, measured by Lunar Prospector and by analysis of returned samples. However, Lunar Prospector Si data contradict the Si content in returned samples (see Fig. 1). The Si content in western maria is significantly lower according to Lunar Prospector results than that measured in returned samples. The underestimation of Si content by 6–10 wt% leads to overestimation of Mg content on 3–4 wt% (see Fig. 2) and Al content on several wt% in Th-rich western maria.

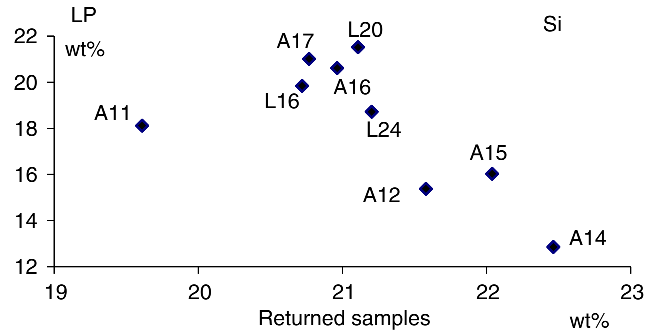

Fig. 1. Comparison between Lunar Prospector measurements of elemental composition of returned sample sites and bulk elemental abundances of returned samples for Si content.

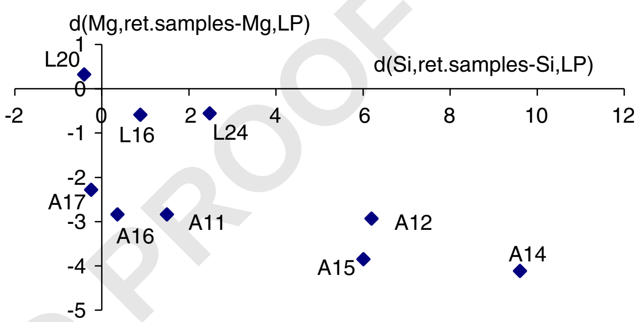

Fig. 2. Difference between Mg content in returned samples and Lunar Prospector measurements of returned samples sites versus the same difference for Si content.

Abundance correlations between several elements were estimated because they are important to create high-resolution maps for other elements based on currently available high-resolution Th, Ti and Fe maps (Shkuratov et al., 2004). Some global correlations for the surface of the Moon, derived from the Lunar Prospector pixel counts, are listed below:

$$\mathrm{U\ (ppm)} = 0.365\mathrm{Th\ (ppm)} + 0.01,\quad r^2 = 0.97,\quad \sigma = 0.1\ \mathrm{ppm}, \tag{1}$$

$$\mathrm{K\ (ppm)} = 344\mathrm{Th\ (ppm)} + 130,\quad r^2 = 0.96,\quad \sigma = 130\ \mathrm{ppm}, \tag{2}$$

$$\mathrm{Al\ (wt\%)} = -0.6\mathrm{Fe\ (wt\%)} + 16.6,\quad r^2 = 0.63,\quad \sigma = 1.6\ \mathrm{wt\%}, \tag{3}$$

$$\mathrm{Mg\ (wt\%)} = 0.41\mathrm{Fe\ (wt\%)} + 2.8,\quad r^2 = 0.51,\quad \sigma = 1.4\ \mathrm{wt\%}, \tag{4}$$

$$\mathrm{Ca\ (wt\%)} = -0.35\mathrm{Fe\ (wt\%)} + 13,\quad r^2 = 0.35,\quad \sigma = 1.7\ \mathrm{wt\%}. \tag{5}$$

Our results agree qualitatively with the previous study of the K–Th relationship based on Lunar Prospector data (Lawrence et al., 1998). Our Al–Fe correlation is similar to that for returned samples,

$$\mathrm{Al\,(wt\%)} = -0.850\mathrm{Fe\,(wt\%)} + 17.4, \quad r^2 = 0.96, \tag{6}$$

and for Apollo orbital X-ray and gamma-ray data,

$$\mathrm{Al\,(wt\%)} = -0.711\mathrm{Fe\,(wt\%)} + 15.7, \quad r^2 = 0.555, \tag{7}$$

as obtained by Spudis et al. (1988).

The correlation coefficients between abundances of Ca, Al, and Mg and Th, Fe, Ti vary between 0.2 and 0.6. Synthetic high-resolution Ca, Al, or Mg maps, produced from Th, Ti, and Fe maps, will have large errors, about 3 wt% at the 2σ level. The correlation coefficients and determination errors were determined by standard regression methods. The correlation between different elements varies between different regions of the Moon. For example, for the north polar region (60–90N), the correlation coefficient between the abundances of Ca and Fe is only 0.02, so for the construction of synthetic Ca, Al, Mg maps it would be better to use regional correlation coefficients of these elements with Th, Fe and Ti.

3. Petrologic maps of the moon

Returned lunar samples contain some principal types of pristine rocks: anorthosites, Mg-suite rocks (troctolites, norites, and dunites among others), KREEP and mare basalts. Maps of elemental abundances permit us to attempt to construct petrologic maps of the Moon. Such maps contain information about the distribution of different rock types on the lunar surface. Metzger and Drake (1990) proposed to search for deposits of rare rock types based on remote sensing data. This approach is not powerful, because the lunar surface is usually covered by a mixture of different rocks. The variety of petrologic provinces on the Moon may be explained by different mixtures of pristine rock types (Davis and Spudis, 1985). The Fe–$(\mathrm{Th/Ti})_c$ diagram ($(\mathrm{Th/Ti})_c$ is Th/Ti ratio normalized to chondrites) is very useful for determination of the abundances of mare basalts, KREEP basalts and ferroan anorthosites (Spudis et al., 2000). However, this diagram cannot discriminate KREEP basalts and Mg-suite rock types. Such a discrimination can be conducted using Al–Mg*/$(\mathrm{Th/Ti})_c$ (Mg* is the Mg-number) and Mg*–$(\mathrm{Th/Ti})_c$ diagrams (Davis and Spudis, 1985, 1987). In these early works, however, the remote geochemical data were limited to equatorial regions.

In our article, we will try to estimate the abundances of Mg-rich rock types, based on Al–Mg and Fe–Mg diagrams. The use of these diagrams has some advantages in comparison with Al–Mg*/$(\mathrm{Th/Ti})_c$ and Mg*–$(\mathrm{Th/Ti})_c$ diagrams, because the two-element approach eliminates the errors resulting from dividing numbers that can have high uncertainties, especially at low concentration. The search for deposits of Mg-rich rock types relates to the Mg abundance on the lunar surface, a map of which is shown in Fig. 3. Let us note that the Mg content varies significantly over the highlands giving evidence of the complex history and heterogeneity of the highland regions. Mg-rich regions (6–9 wt% Mg) in highlands, which can contain troctolites, norites and gabbronorites, are located in the South Pole Aitkin basin.

Al can be used for distinguishing between mare basalts and highland rocks (see Fig. 4). A Lunar Prospector Fe map for the Moon has already been published by Lawrence et al. (2002).

Al–Mg and Fe–Mg diagrams allow us to discriminate KREEP basalts and Mg-rich rocks well (see Figs. 5 and 6). The initial elemental composition of end members was taken from Phillips (1986). Then the final elemental composition of end members was determined by minimization of distances of observed data pixels from the three end-member plane in Mg–Fe–Al space. Namely, ferroan anorthosites are taken to contain 0.5 wt% Mg, 17.3 wt% Al, 1 wt% Fe, mare basalts to contain 5 wt% Mg, 5 wt% Al, 17.8 wt% Fe, and Mg-rich rocks to have a composition similar to that of troctolites containing 13.2 wt% Mg, 12 wt% Al, 5 wt% Fe. Let us note that abundances of Mg-rich rocks may be overestimated due to the overestimation of Lunar Prospector Mg content in western maria. In our research impact glasses are not considered, while they are abundant in some lunar regions, because their elemental composition strongly depends on their origin. For a study of abundances of impact glasses, 25Ti–5(Fe–Ti)–Al petrologic diagrams were used by Zellner et al. (2002). It is difficult to distinguish different Mg-rich rock types on our diagrams. For example, Mg-suite rocks have chemical properties as primitive (for example, high Mg-number) as evolved magmatic (for example, high content of incompatible trace elements). There are also some rocks which are Mg-rich, but do not belong to the Mg-suite group. A mixture of ferroan anorthosite with troctolite would have the same Mg content as a pure norite deposit.

The relative abundances of mare basalts, Mg-rich rocks and ferroan anorthosites are plotted in ternary space for each pixel on the lunar surface. Primary colors red, blue, and green are assigned for the end-member classes of mare basalts, ferroan anorthosites, and Mg-rich rocks, respectively. The ternary space defined by these points is represented by the mixture of these primary colors.

The map of abundances of ferroan anorthosites, mare basalts and Mg-rich rocks based on Fe and Mg content is shown in Fig. 7. The nearside maria are regions with a

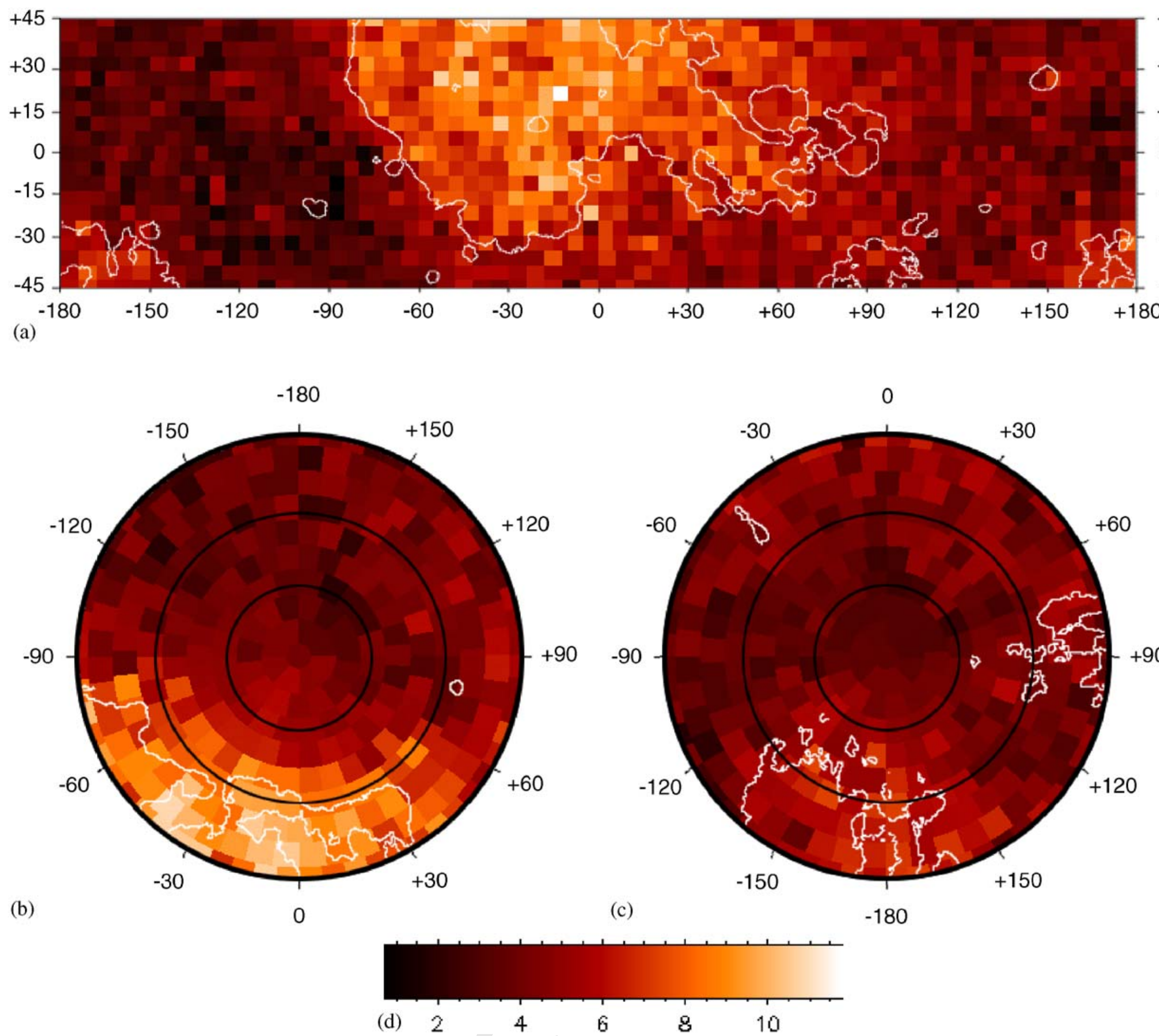

Fig. 3. Map of Mg abundance on the Moon. (a) Equatorial regions, (b) north polar region, (c) south polar region. Albedo contours are taken from Clementine data (Lucey et al., 1994).

high content of mare basalts as expected. The majority of highland regions contain ferroan anorthosites and Mg-rich rocks with a small amount of mare basalts. Our results agree well with the petrologic map obtained by Spudis et al. (2000). This demonstrates the suitability of our approach for representing petrologic provinces on the Moon. The distribution of Mg-rich rocks on our map is almost the same as the distribution of Mg-suite rocks and KREEP basalts on the map by Spudis et al. (2000). This means that KREEP basalts are not so abundant in comparison with Mg-rich rocks on the lunar surface. However, KREEP basalts are abundant in Th-rich region, located in the western maria. Unfortunately, incorrect estimation of Mg and Si content in this region leads to incorrect estimation of the end-member abundances here. Mg-rich rocks are located in the Mare Frigoris region, at the edges of big maria, and in some cryptomaria such as the Copernicus cryptomare, the Balmer basin, the Gartner-Atlas region, and the region of dark halo craters near crater Alphonsus. Suggesting the presence of Mg-rich rocks in Mare Frigoris, we can explain some unique features of this mare in comparison with other maria, such as the Fe and Ti depletion discussed by Taylor et al. (1996). Mg-rich rocks are also abundant in highlands (they are shown by a light blue color here), especially in the nearside south (20–60S) and polar north (70–90N) regions, and east from Mare Serenitatis. These results agree well with the study of Mg-number distribution on the Moon (Prettyman et al., 2002b). Let us note that norites and gabbronorites generally have a lower Ca content in comparison with ferroan anorthosites and troctolites. Thus, Ca mapping on the Moon is useful for studying these rock types. The Ca content is significantly lower in the nearside highlands than in the farside highlands. This is an additional fact confirming the presence of Mg-rich rocks such as norites and gabbronorites in the nearside highlands.

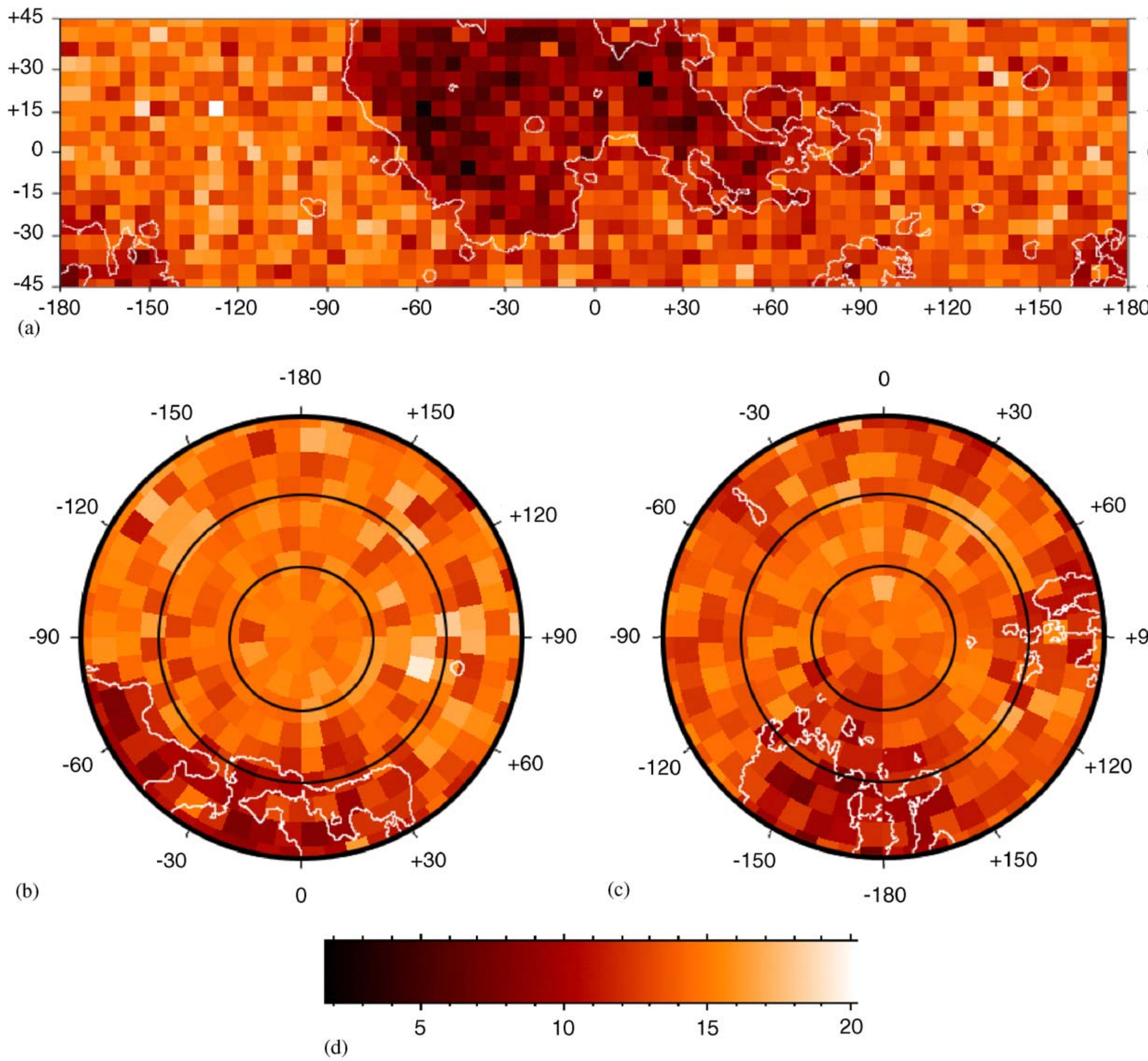

Fig. 4. Map of Al abundance on the Moon. (a) Equatorial regions, (b) north polar region, (c) south polar region. Albedo contours are taken from Clementine data (Lucey et al., 1994).

Cryptomaria are ancient mare basalts deposits: their age is more than 3.8 billion years. It is difficult to study cryptomaria by optical and near-infrared spectroscopy due to mixing of ancient deposits with younger higher albedo material. By using Apollo X-ray spectrometer data, cryptomaria were detected in highlands (Schultz and Spudis, 1979, 1983). Different types of remote sensing data have been used for the study of ancient lunar volcanism (Hawke and Spudis, 1980; Hawke et al., 1985). Our study confirms the presence of mare basalts in the majority of known cryptomaria: the Lomonosov–Fleming basin, the Schillerd–Schickard, Mendel–-Rydberg regions, and in the Janssen (50S, 40 E) region also. This possible cryptomare is seen only as a two-pixel region on 150 km spatial resolution map. The Al abundance is lower in this region in comparison with the surrounding areas, suggesting the possible detection of a cryptomare. However, the Fe and Mg contents in the Janssen region are similar and lower, respectively, in comparison with the surrounding areas: these data contradict the cryptomare hypothesis.

The petrologic map constructed from Al and Mg abundances (see Fig. 8) generally agrees with that based on Fe and Mg abundances. Cryptomaria can also be seen on the Mg–Al petrologic map. If the three end-member hypothesis is correct, the colors on both the Fe–Mg and Al–Mg maps should be the same. However, there are some regions showing different colors on these maps. This fact is evidence of the presence of rocks with a different elemental composition from the end-member rocks. According to the Al–Mg map, mare basalts and Mg-rich rocks are more abundant in the highlands than the Fe–Mg map indicates. This fact can be explained by the presence of norites (4 wt% Fe, 4–7 wt% Mg, 8–13 wt% Al). The South Pole Aitken basin has an intermediate elemental composition between the three

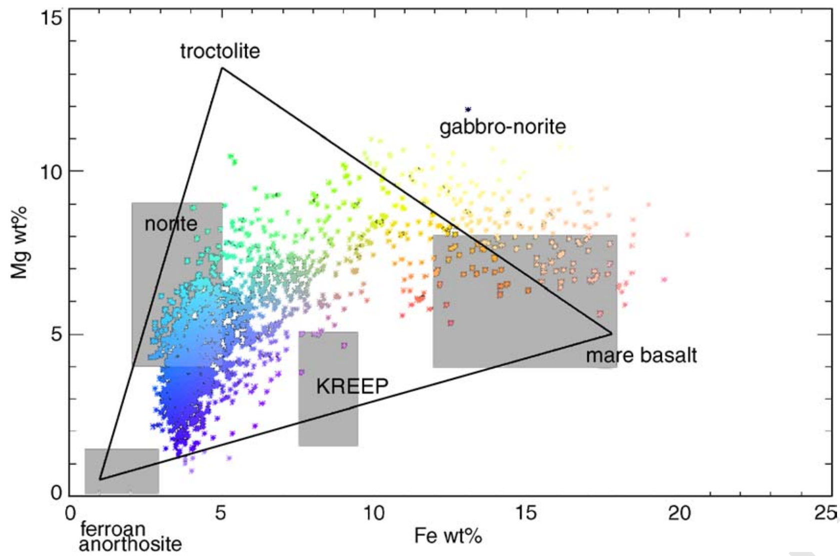

Fig. 5. Scattergram shows Lunar Prospector gamma-ray spectrometer data for 5 degree squares in Mg–Fe compositional space. Mg and Fe abundances in different rock types are taken from Phillips (1986).

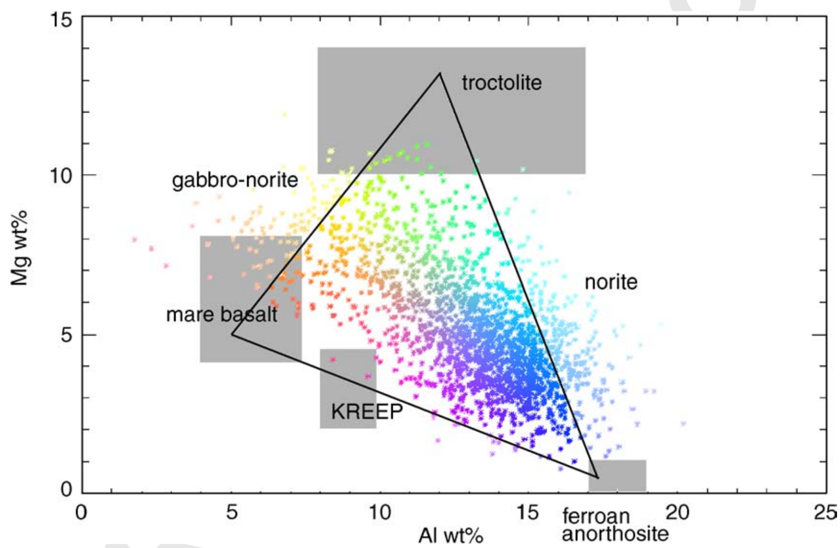

Fig. 6. Scattergram shows Lunar Prospector gamma-ray spectrometer data for 5 degree squares in Al–Mg compositional space. Al and Mg abundances in different rock types are taken from Phillips (1986).

rock end-members. A large disagreement between the colors of the maps also occurs in the South Pole Aitken basin, this is evidence of the presence of some rare rock types here. The presence of Mg-rich rocks in this basin can be explained by Mg-rich rocks being more abundant in the lower crust than in the upper crust. While we choose troctolites (9–16 wt% Al, 10–19 wt% Mg, 4–6 wt% Fe, 11–15 wt% Ca) as the third end-member rock, there are no 150 km regions on the Moon with the troctolite elemental composition. Our results agree well with the study of Pieters and Tompkins (1999), in which troctolites were detected only in kilometer size regions in central peaks of some craters. However, gabbronorites (4–9 wt% Al, 2–16 wt% Mg, 8–13 wt% Fe, 4–8 wt% Ca) are more abundant on the lunar surface. There are about 20 pixels with the gabbronorite elemental composition, especially at the edges of eastern maria.

Knowing the elemental abundances on the Moon, it is possible to search for rare rock types. For example, dunites have extremely high Mg (25 wt%) and extremely low Ca (1 wt%) and Al (1 wt%) abundances. There are no regions on the Moon with dunites elemental composition. The regions with lowest Al (3–7 wt%) and Ca (~5 wt%) abundances (the Reiner crater region at 12N, 55W and the center of Mare Tranquilitatis at 10N, 25E) have moderate Mg content (about 8 wt%).

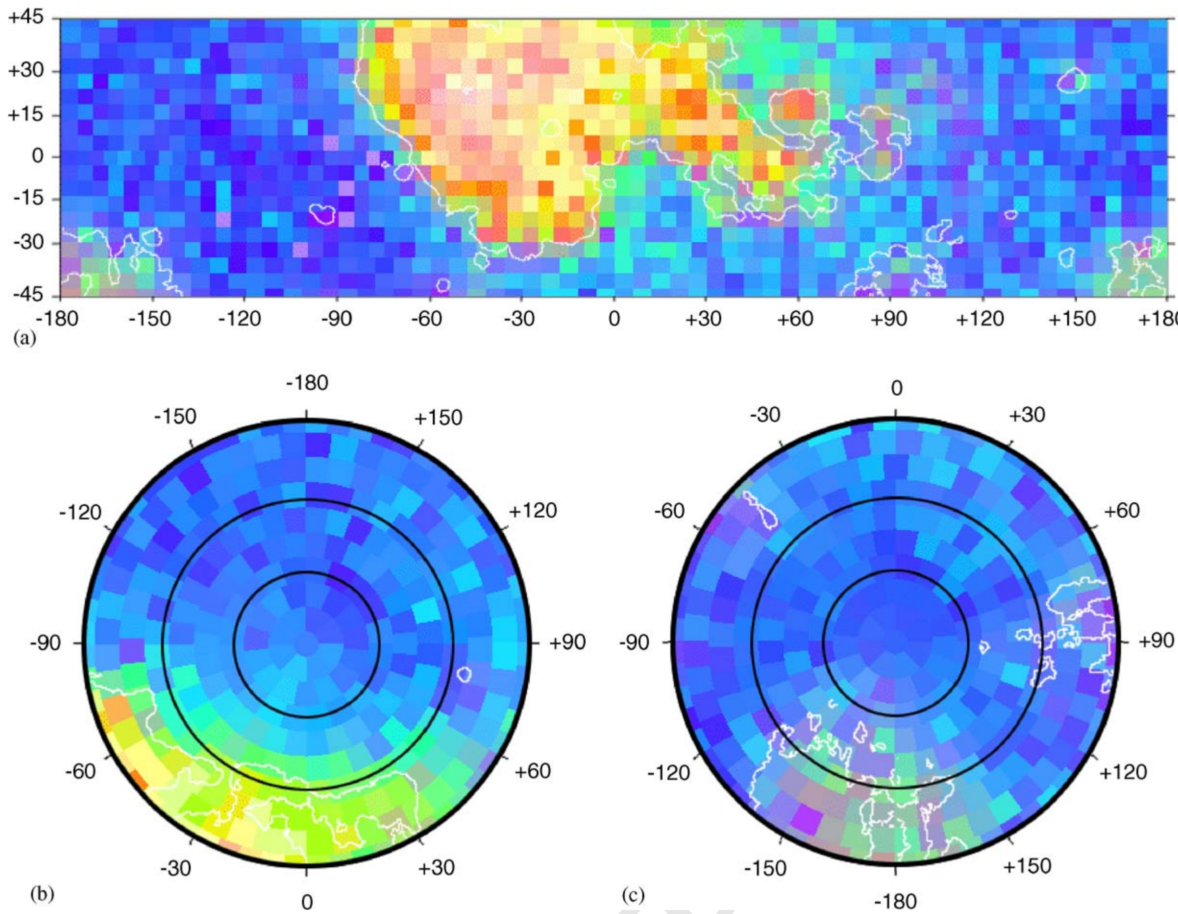

Fig. 7. Petrologic map of the Moon based on Fe and Mg Lunar Prospector data. (a) Equatorial regions, (b) north polar region, (c) south polar region. Albedo contours are taken from Clementine data (Lucey et al., 1994).

The region with highest Mg abundance (12 wt%), located near the Copernicus crater, has moderate Ca (9 wt%) and Al (7 wt%) abundances. Many other rock types do not have such sharply distinguishable properties. For example, aluminous mare basalts have an intermediate elemental composition between Fe-rich mare basalts and ferroan anorthosites. It is difficult to separate aluminous basalts from mixing components at such low spatial resolution.

Pyroclastic deposits are important for the study of mare volcanism on the Moon. Pyroclastic deposits were first mapped by their high Mg/Al ratios with usage of Apollo X-ray data by Schonfeld and Bielefeld (1978). They can also be studied by analysis of lunar reflectance spectra (Gaddis et al., 1985; Hawke et al., 1989). Our study of Lunar Prospector data shows that a very high Mg/Al ratio, higher than 1.5, is typical for regions with Al content less than 6 wt%. Such regions are located near Reiner crater in Oceanus Procellarum, at the north part of Mare Imbrium, and in other maria (see Fig. 9). Let us note that the existence of one pixel anomaly at 25N, 18E with very low Al content equal to 1.8 wt% may be error. Only the biggest pyroclastic deposit region in the Aristarchus plateau shows a high Mg/Al ratio equal to 1.4. This region may be distinguished from other high Mg/Al ratio regions by its higher Th and Ti content (6.5 ppm and 3.2 wt%, respectively). Other pyroclastic deposits have an Mg/Al ratio less than unity: they are too small (less than 10,000 km^2) for a significant increase of the Mg/Al ratio even for one Lunar Prospector data pixel (about 22,000 km^2). The Mg/Al ratio will be more useful for the study of pyroclastic deposits when Mg and Al data with better spatial resolution are available.

4. Limitations of three end-member hypothesis and four end-member model

If the three end-member hypothesis is correct and statistical errors are negligible, then abundances of end members in each pixel, determined by Mg–Fe and Mg–Al approaches, should be the same. However, the abundances of end members, determined by Mg–Al and Mg–Fe contents, are different due to the presence of rocks with different elemental compositions from the

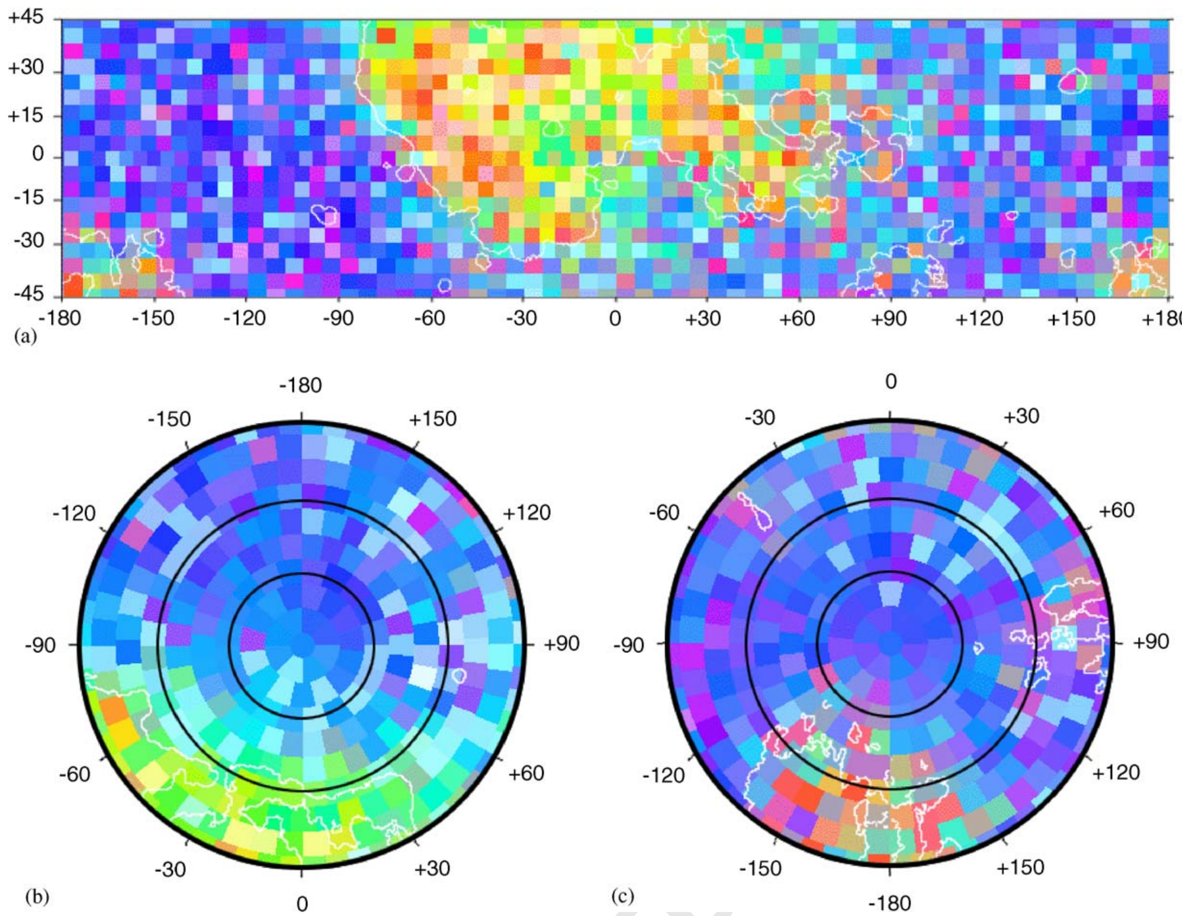

Fig. 8. Petrologic map of the Moon based on Al and Mg Lunar Prospector data. (a) Equatorial regions, (b) north polar region, (c) south polar region. Albedo contours are taken from Clementine data (Lucey et al., 1994).

end-member rocks and due to the existence of errors of estimation of elemental abundances. The degree of the difference between real rock composition and mixture of rock members is proportional to the distance of pixels from three end-member plane. In our case, this distance ρ (in wt%) is equal to

$$\rho = -0.552\mathrm{Fe}(x) - 0.816\mathrm{Al}(x) - 0.167\mathrm{Mg}(x) + 14.76, \quad (8)$$

where Fe(x), Al(x), and Mg(x) are Fe, Al, and Mg contents in a given Lunar Prospector pixel. Knowing the elemental composition of three end members (three points), it is possible to find the equation of the three end-member plane, because these three points belong to a unique plane. Then the distance between a point and the plane in three-dimensional space is determined by methods of analytical geometry. Coefficients at Fe(x), Al(x) and so on can be found from the equation of the three end-member plane. Thus, negative values of ρ mean that Fe, Al, or Mg content in a pixel are higher than that in a mixture of end-member rocks, while positive ρ values mean underestimation of Fe, Al, or Mg content in comparison with end members.

The biggest region with negative ρ values is located in the western maria (see Fig. 10). This region has almost the same location as the region with very low Si content. This means that the appearance of this region on a ρ value map can be explained by overestimation of Mg and Al content, caused by underestimation of Si content. While elemental composition of western maria is comparable with that of norites, an incorrect estimation of Mg and Si content in this region reduces the likelihood of the presence of norites there.

Pixels with maximal positive values are located mainly in the farside highlands (see Table 1). These regions are shown as violet pixels on the Al–Mg map and as light blue pixels on the Fe–Mg map. The size of these anomalies is less than 150 km, because they occur as one-pixel anomalies on Lunar Prospector elemental maps. Such regions have higher Ca (14–17 wt%) and Fe (~4 wt%) content, lower Al (10–12 wt%) and O (43–45 wt%) content in comparison with surrounding areas, and do not differ from them in Mg (~4 wt%) and other element content. These data show the existence of a Ca-rich rock type. The moderately high Fe content in these regions can be explained by the younger age of this rock type in comparison with ferroan anorthosites.

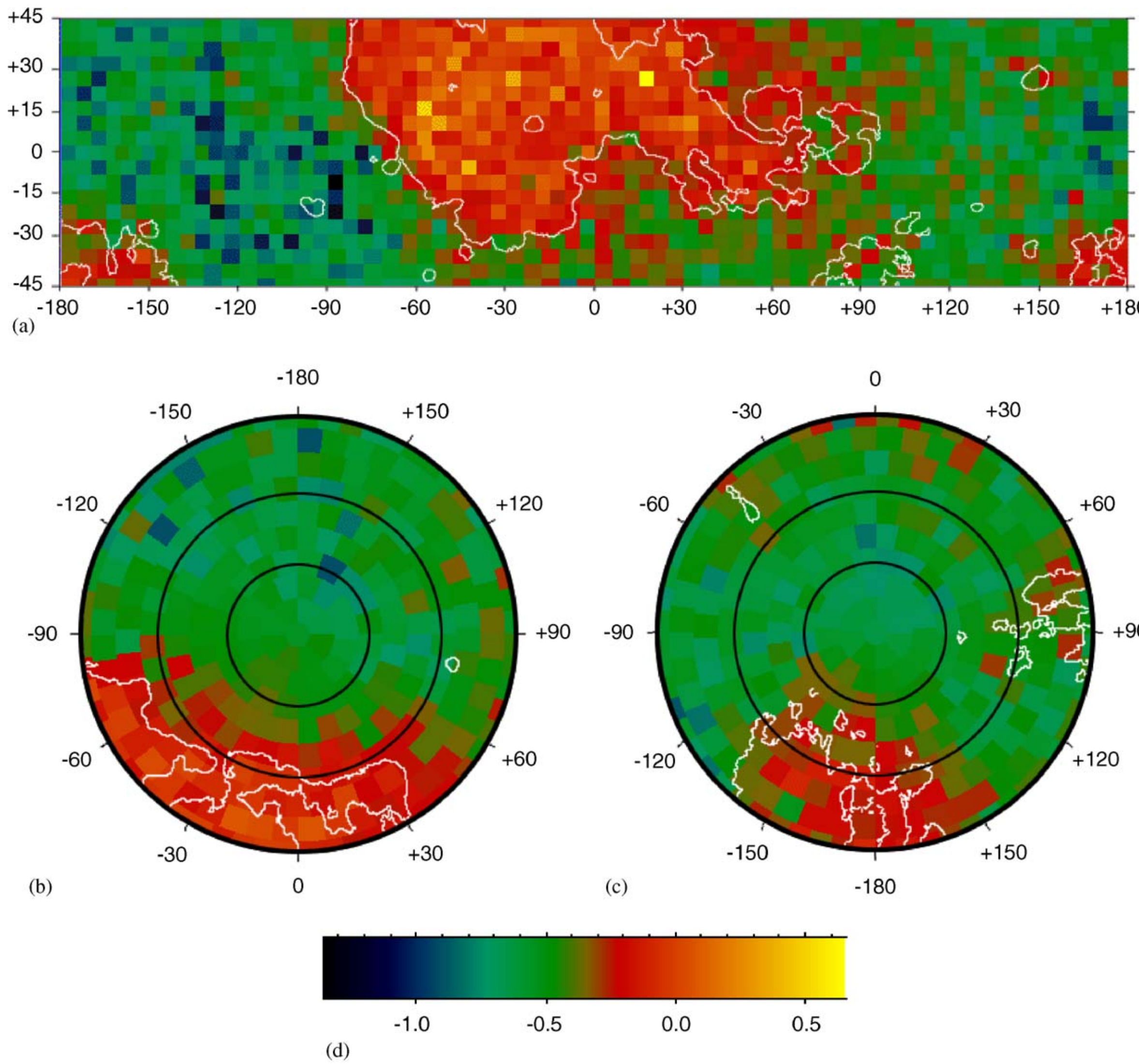

Fig. 9. Map of logarithm of Mg/Al ratio on the Moon. (a) Equatorial regions, (b) north polar region, (c) south polar region. Albedo contours are taken from Clementine data (Lucey et al., 1994).

The map of ρ values on the Moon is useful for improvement of the three end-member model. For example, the addition of KREEP basalts as a fourth end-member is desirable for better representation of the Th-rich region in the western maria. However, the Mg–Al–Fe petrologic technique cannot be used for adding a fourth end-member, because Mg, Al, Fe Lunar Prospector data in western maria contradict the presence of KREEP basalts here. An Mg–Th–Fe petrologic technique is more useful than the Mg–Al–Fe technique for the development of a four end-member model due to the higher quality of Th data in comparison with Al data. Let us assume that KREEP basalts contain 4 wt% Mg, 8 wt% Fe, and 20 ppm Th and ferroan anorthosites, mare basalts, and Mg-rich rocks contain 0.1 ppm Th, 0.5 ppm Th, 1 ppm Th, respectively, according to Phillips (1986). Let us choose ferroan anorthosites, mare basalts, and KREEP basalts as end members. Then the distance ρ of Lunar Prospector pixels from three end-member plane determined by standard methods of analytical geometry is equal to

$$\rho = 0.256\mathrm{Fe}(x) + 0.0793\mathrm{Th}(x) - 0.963\mathrm{Mg}(x) + 0.218, \tag{9}$$

where Fe(x), Th(x), and Mg(x) are the Fe, Th, and Mg contents in a given Lunar Prospector pixel. The ρ values are negative for majority of the lunar surface due to the presence of Mg-rich rocks. The correlation coefficient between the distance of pixels from three end-member plane in Fe–Th–Mg compositional space and Mg-rich rocks content, determined by Al–Mg technique, is high enough ($r^2 \sim 0.8$) for the addition of Mg-rich rocks as fourth end-member. Correlations between abundances

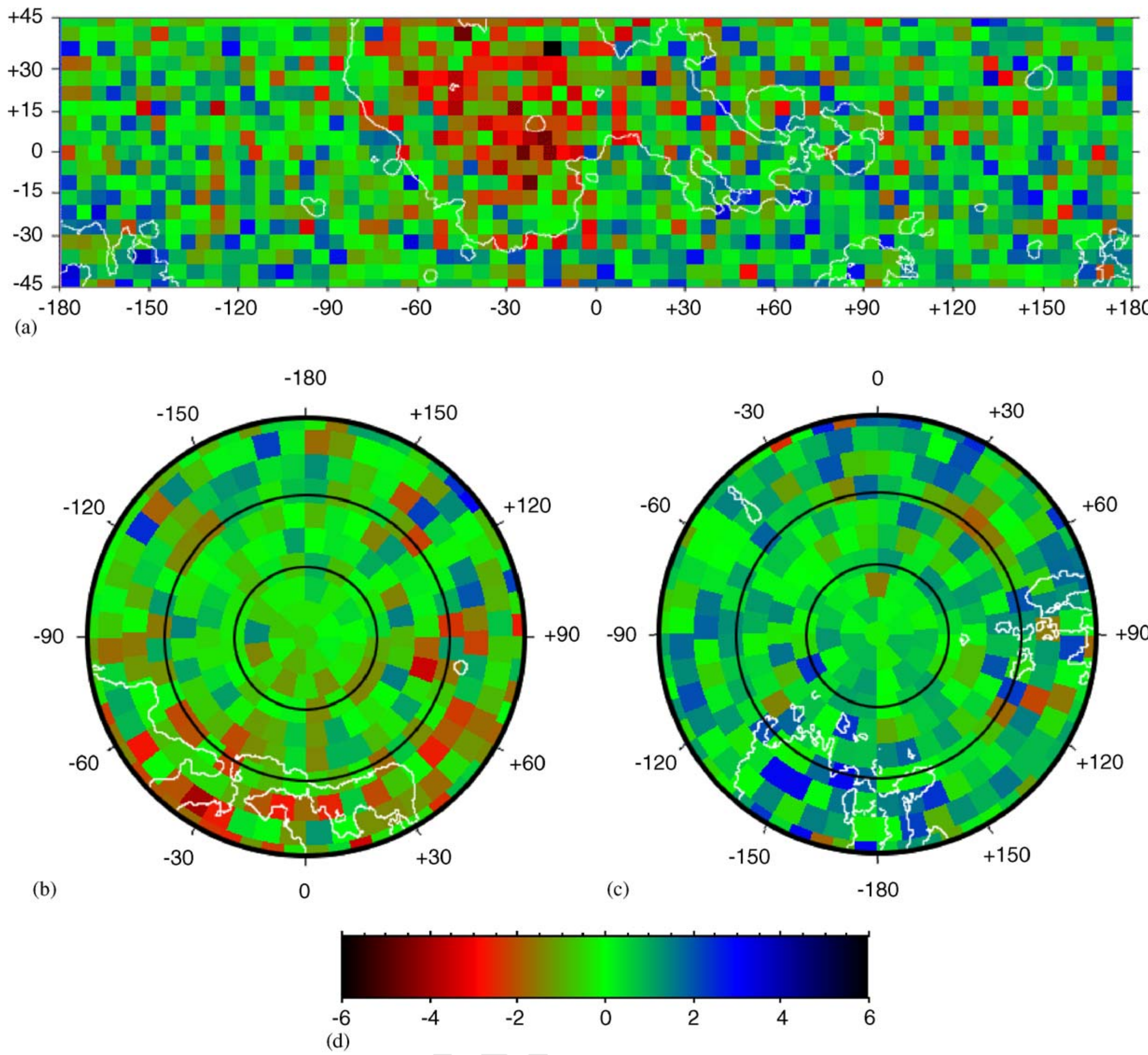

Fig. 10. Map of the distances of Lunar Prospector pixels from the three end-member plane in Mg–Al–Fe space. (a) Equatorial regions, (b) north polar region, (c) south polar region. Albedo contours are taken from Clementine data (Lucey et al., 1994).

Table 1
Elemental composition of highland regions with high Ca content

Latitude	Longitude	Ca (wt%)	Al (wt%)	Fe (wt%)	Mg (wt%)	Distance from three end-member plane (wt%)
37.5–42.5S	102–108W	15.1	10.9	4.4	3.6	2.8
32.5–37.5S	96–102W	14.3	12.9	4	2.2	1.7
32.5–37.5S	30–36E	13.2	10	4.8	4.1	3.3
27.5–32.5S	120–125W	14.4	12	3.8	1.7	2.6
17.5–22.5N	160–165W	16.4	11.6	4.1	3.5	2.4
22.5–27.5N	145–150W	17.5	12.5	3.9	3.3	1.9
27.5–32.5N	140–145E	14.6	9.9	4.6	5.8	3.2
27.5–32.5N	155–160E	13.3	10.6	5	4.5	2.6
32.5–37.5N	174–180W	14.4	10.7	4	3.5	3.2
32.5–37.5N	120–126W	14.7	10.5	4.7	3.9	3
32.5–37.5N	126–132E	16	12.4	4.6	2.6	1.7
42.5–47.5N	126–132E	14.5	10.5	4.2	4.7	3.1
47.5–52.5N	165–172.5W	15	11.7	3.9	4.7	2.3
47.5–52.5N	120–127.5W	14	11.3	4.1	4.8	2.5
52.5–57.5N	100–108E	13.4	12.3	3.7	4.3	2
52.5–57.5N	132–140E	14.8	11.9	4.2	3.4	2.2

of ferroan anorthosites and Mg-rich rocks, determined by Fe–Mg–Th and Al–Mg petrologic techniques, are strong (r^2~0.8), it confirms the suitability of Fe–Mg–Th approach. Correlation is not so strong for mare basalts content (r^2~0.5), because KREEP basalts as the new end-member are abundant in mare regions.

However, the use of a four end-member model has a little advantage in comparison with simpler three end-member model due to the existence of errors in Lunar Prospector data for Th-rich regions. The spatial resolution of the four end-member technique is equal to only 150 km, while KREEP basalts can be mapped with 15 km pixel size, based on available high-resolution Th data. When more accurate elemental data with better spatial resolution will be available, the Fe–Th–Mg petrologic technique will be useful and it will be possible to use a Mg–Al–Fe–Th technique for the determination of abundances of five end members (ferroan anorthosites, mare basalts, KREEP basalts, two different types of Mg-rich rocks).

5. Conclusions

By comparison of the elemental composition of landing sites measured by Lunar Prospector with returned sample analysis, it was found that the Si content is underestimated and the Mg, Al content is overestimated by Lunar Prospector in Th-rich western maria. Correlations between the abundances of different elements on the lunar surface have been investigated using Lunar Prospector data. The best correlations occur for Th, K, and U distributions (r^2~0.95). It is possible to create K and U high-resolution maps based on the available high-resolution Th map. The correlations between other major elements are not so strong (r^2~0.2–0.6). A study of Ca content on the Moon is useful for the estimation of abundances of norites, gabbronorites, ferroan anorthosites, and troctolites.

With the use of Al–Mg and Fe–Mg diagrams, petrologic maps of the Moon have been built. Our results of a search for mare basalts in the lunar highlands agree well with previously published data. Among the most interesting results is the detection of Mg-rich rocks in the Mare Frigoris region. Mg-rich rocks deposits were found also in some cryptomaria and at the edges of large maria. The biggest pyroclastic deposit in the Aristarchus plateau was found by its high Mg/Al ratio. The study of pyroclastic deposits will be more fruitful when Mg and Al data with better spatial resolution are obtained.

Comparison of the Al–Mg and Fe–Mg petrologic maps allows us to indicate the limitations of the simple three end-member model and to determine regions where other rock types are abundant. For example, poorly known rock types are abundant in the South Pole Aitken basin, and norites are abundant in the highlands.

The study of Lunar Prospector data in Mg–Al–Fe space is also suitable for checking the three end-member model. Small-area Ca-rich anomalies having higher Fe and lower Al and O content in comparison with neighboring regions are found in the farside highlands. The quality of Lunar Prospector Mg, Al, Fe data is not sufficient for adding KREEP basalts as the fourth end-member to Mg–Al–Fe petrologic model. An Mg–Th–Fe petrologic technique can be used for simultaneous determination of KREEP basalts and Mg-rich rock content as different end members, when the errors of estimation of Mg content in Th-rich regions are improved.

Acknowledgments

A.A. Berezhnoy is supported by a postdoctoral fellowship Grant (No. P02059), provided by the Japanese Society for the Promotion of Science (JSPS). G. Michael acknowledges the European Community's Human Potential Programme under contract RTN2-2001-00414, MAGE. We acknowledge two anonymous referees: their remarks helped us to improve this paper.

References

Davis, P.A., Spudis, P.D., 1985. Petrologic province maps of the lunar highlands derived from orbital geochemical data. J. Geophys. Res. 90, D61–D74.

Davis, P.A., Spudis, P.D., 1987. Global petrologic variations on the Moon—a ternary-diagram approach. J. Geophys. Res. 92 (B4), 387–395.

Dunkin, S.K., Grande, M., Casanova, I., Fernandes, V., Heather, D.J., Kellett, B., Muinonen, K., Russell, S.S., Browning, R., Waltham, N., Parker, D., Kent, B., Perry, C.H., Swinyard, B., Perry, A., Feraday, J., Howe, C., Phillips, K., McBride, G., Huovelin, J., Muhli, P., Hakala, P.J., Vilhu, O., Thomas, N., Hughes, D., Alleyne, H., Grady, M., Lundin, R., Barabash, S., Baker, D., Clark, P.E., Murray, C.D., Guest, J., d'Uston, L.C., Maurice, S., Foing, B., Christou, A., Owen, C., Charles, P., Laukkanen, J., Koskinen, H., Kato, M., Sipila, K., Nenonen, S., Holmstrom, M., Bhandari, N., Elphic, R., Lawrence, D., 2003. Scientific rationale for the D-CIXS X-ray spectrometer on board ESA's SMART-1 mission to the Moon. Planet. Space Sci. 51, 435–442.

Elphic, R.C., Lawrence, D.J., Feldman, W.C., Barraclough, B.L., Maurice, S., Binder, A.B., Lucey, P.G., 2000. Lunar rare earth element distribution and ramifications for FeO and TiO_2: Lunar Prospector neutron spectrometer observations. J. Geophys. Res. 105, 20333–20345.

Gaddis, L.R., Pieters, C.M., Hawke, B.R., 1985. Remote sensing of lunar pyroclastic mantling deposits. Icarus 61, 461–489.

Hawke, B.R., Spudis, P.D., 1980. Geochemical anomalies on the eastern limb and farside of the moon. In: Proceedings of Conference on the Lunar Highlands Crust, pp. 467–481.

Hawke, B.R., Spudis, P.D., Clark, P.E., 1985. The origin of selected lunar geochemical anomalies: implications for early volcanism and the formation of light plains. Earth Moon Planets 32, 257–273.

Hawke, B.R., Coombs, C.R., Gaddis, L.R., Lucey, P.G., Owensby, P.D., 1989. Remote sensing and geologic studies of localized dark mantle deposits on the moon. In: Proceedings of 19th Lunar and Planetary Science Conference, pp. 255–268.

Keller, H.U., Mall, U., Nathues, A., 2001. Mapping the Moon With SIR, an infrared spectrometer for SMART-1. Earth Moon Planets 85/86, 545.

Kobayashi, M.N., Hasebe, N., Miyachi, T., Doke, T., Kikuchi, J., Okada, H., Oka, A., Okudaira, O., Souri, H., Yamashita, N., Shibamura, E., Kashiwagi, T., Takashima, T., Narasaki, K., Tsurumi, K., Mori, K., D'Uston, C., Maurice, S., Grande, M., Reedy, R.C., 2002. High-purity germanium gamma-ray spectrometer with stirling cycle cryocooler. Adv. Space Res. 30, 1927–1931.

Lawrence, D.J., Feldman, W.C., Barraclough, B.L., Binder, A.B., Elphic, R.C., Maurice, S., Thomsen, D.R., 1998. Global elemental maps of the Moon: the Lunar Prospector gamma-ray spectrometer. Science 281, 1484–1489.

Lawrence, D.J., Feldman, W.C., Barraclough, B.L., Binder, A.B., Elphic, R.C., Maurice, S., Miller, M.C., Prettyman, T.H., 2000. Thorium abundances on the lunar surface. J. Geophys. Res. 105 (E8), 20307–20331.

Lawrence, D.J., Feldman, W.C., Elphic, R.C., Little, R.C., Prettyman, T.H., Maurice, S., Lucey, P.G., Binder, A.B., 2002. Iron abundances on the lunar surface as measured by the Lunar Prospector gamma-ray and neutron spectrometers. J. Geophys. Res. 107 (E12), 1–13 (CiteID 5130).

Lawrence, D.J., Elphic, R.C., Feldman, W.C., Prettyman, T.H., Gasnault, O., Maurice, S., 2003. Small-area thorium features on the lunar surface. J. Geophys. Res. 108 (E9), 1–6 (CiteID 5102).

Lucey, P.G., 2004. Mineral maps of the Moon. Geophys. Res. Lett. 31 (CiteID L08701).

Lucey, P.G., Spudis, P.D., Zuber, M., Smith, D., Malaret, E., 1994. Topographic compositional units on the Moon and the early evolution of the lunar crust. Science 266, 1855–1858.

Lucey, P.G., Blewett, D.T., Hawke, B.R., 1998. Mapping the FeO and TiO_2 content of the lunar surface with multispectral imagery. J. Geophys. Res. 103 (E2), 3679–3700.

McCord, T.B., Clark, R.N., Hawke, B.R., McFadden, L.A., Owensby, P.D., Pieters, C.M., Adams, J.B., 1981. Moon—near-infrared spectral reflectance, a first good look. J. Geophys. Res. 86, 10883–10892.

Metzger, A.E., Drake, D.M., 1990. Identification of lunar rock types and search for polar ice by gamma-ray spectroscopy. J. Geophys. Res. 95 (B1), 449–460.

Okada, T., Kato, M., Yamashita, Y., Shirai, K., Yamamoto, Y., Matsuda, T., Tsunemi, H., Kitamoto, S., 2002. Lunar X-ray spectrometer experiment on the SELENE mission. Adv. Space Res. 30, 1909–1914.

Phillips, R. (Ed.), 1986. LGO Science Workshop, Contributions of a Lunar Geoscience Observer Mission to Fundamental Questions in Lunar Science. Department of geological sciences, Southern Methodist University, Dallas, Texas.

Pieters, C.M., Tompkins, S., 1999. The Distribution of Lunar Olivine/Troctolite Outcrops: Mineralogical Evidence for Mantle Overturn? Lunar Planet. Sci. Conf. 30, 1286.

Prettyman, T.H., Feldman, W.C., Lawrence, D.J., McKinney, G.W., Binder, A.B., Elphic, R.C., Gasnault, O.M., Maurice, S., Moore, K.R., 2002a. Library least squares analysis of Lunar Prospector gamma-ray spectra. Lunar Planet. Sci. Conf. 33, 2012.

Prettyman, T.H., Lawrence, D.J., Vaniman, D.T., Elphic, R.C., Feldman, W.C., 2002b. Classification of Regolith Materials from Lunar Prospector Data Reveals a Magnesium-Rich Highland Province, The Moon Beyond 2002: Next Steps in Lunar Science and Exploration, p. 49.

Schonfeld, E., Bielefeld, M.J., 1978. Correlation of dark mantle deposits with high Mg/Al ratios. Proceedings of the Ninth Lunar and Planetary Science Conference, vol. 3, pp. 3037–3048.

Schultz, P.H., Spudis, P.D., 1979. Evidence for ancient mare volcanism. Proceedings of 10th Lunar and Planetary Science Conference, vol. 3, pp. 2899–2918.

Schultz, P.H., Spudis, P.D., 1983. Beginning and end of lunar mare volcanism. Nature 302, 233–236.

Shkuratov, Y.G., Stankevich, D.G., Kaydash, V.G., Omelchenko, V.V., Pieters, C.M., Pinet, P.C., Chevrel, S.D., Daydou, Y.H., Foing, B.H., Sodnik, Z., Josset, J.-L., Taylor, L.A., Shevchenko, V.V., 2003. Composition of the lunar surface as will be seen from SMART-1: a simulation using Clementine data. J. Geophys. Res. 108 (E4), 1 (CiteID 5020).

Shkuratov, Y., Pinet, P., Omelchenko, V., Kaydash, V., Stankevich, D., Chevrel, S., Daydou, Y., 2004. Derivation of elemental abundance maps at 15-km spatial resolution from the merging of Clementine optical and Lunar Prospector geochemical data. Lunar Planet. Sci. Conf. 35, 1162.

Spudis, P.D., Davis, P.A., Pattanaborwornsak, B., 1988. The Fe–Al relation of lunar soils and orbital chemical data: Implications for Al abundances estimated from Apollo Orbital gamma-ray data. Lunar Planet. Sci. Conf. 19, 1113–1114.

Spudis, P.D., Bussey, D.B.J., Gillis, J.J., 2000. Petrologic mapping of the Moon from Clementine and Lunar Prospector Data: incorporation of new thorium data. Lunar Planet. Sci. Conf. 31, 1414.

Taylor, G.J., Lucey, P.G., Hawke, B.R., Spudis, P.D., 1996. Composition of the Lunar Maria. Lunar Planet. Sci. Conf. 27, 1317–1318.

Zellner, N.E.B., Spudis, P.D., Delano, J.W., Whittet, D.C.B., 2002. Impact glasses from the Apollo 14 landing site and implications for regional geology. J. Geophys. Res. 107, 11–12 (CiteID 5102).